

The dynamics of a driven harmonic oscillator coupled to pairwise interacting Ising spins in random fields

Paul Zech, Andreas Otto, and Günter Radons

Institute of Physics, Chemnitz University of Technology, Germany.

(Dated: June 13, 2022)

In general we are interested in dynamical systems coupled to complex hysteresis. Therefore as a first step we investigated recently the dynamics of a periodically driven damped harmonic oscillator coupled to independent Ising spins in a random field. Although such a system does not produce hysteresis, we showed how to characterize the dynamics of such a piecewise-smooth system, especially in the case of a large number of spins [P. Zech, A. Otto, and G. Radons, *Phys. Rev. E* 101, 042217 (2020)]. In this paper we extend our model to spin dimers, thus spins with pairwise interactions. We show in which cases two interacting spins can show elementary hysteresis and we give a connection to the Preisach model, which allows us to consider an infinite number of spin-pairs. This thermodynamic limit leads us to a dynamical system with an additional hysteretic force in the form of a play operator. By using methods from general chaos theory, piecewise-smooth system theory and statistics we investigate the chaotic behavior of the dynamical system for a few spins and also in case of a larger number of spins by calculating bifurcation diagrams, Lyapunov exponents, fractal dimensions and self-averaging properties. In doing so, we show, how the dynamical properties of the piecewise-smooth system for a large number of spins differs from the system in its thermodynamic limit.

I. INTRODUCTION

Hysteresis phenomena can occur in many different fields, such as magnetic materials, elastics rubbers, liquid crystals or economy. The investigation of hysteretic systems is an ongoing field of research. For example, hysteresis plays a crucial role in the control of skyrmions via a strain-mediated magnetoelectric coupling [1], in non-monotonic field and temperature responses of magnetic superconductors [2] or in the development of new high coercivity magnets [3].

Many of the existing studies on hysteresis are related to the input-output behavior of hysteresis operators [4–8] or Ising like spin models [9–13]. On the other hand, hysteresis operators can be coupled to dynamical systems leading to a closed-loop dynamical system with hysteresis. In most of the works related to these systems, hysteresis is described by a bi-stable unit leading to a single elementary hysteresis loop in the input-output representation of the hysteresis operator. This kind of hysteresis is known as “simple” hysteresis. For example, there are some results on the conditions for global stability in systems with relay feedback [14], on multistability and hidden attractors in a DC/DC converter with hysteretic relay control [15] as well as results on systems with delayed relay control [16].

A superposition of many elementary hysteresis loops or relays leads to the prominent Preisach Model (PM) [17], which is suitable for describing systems with “complex” hysteresis. “Complex” hysteresis is characterized by one major hysteresis loops and infinitely many inner subloops in the input output representation [18]. Examples for dynamical systems with “complex” hysteresis can be found in robot arm dynamics [19], in the ferroresonance phenomena in LCR circuits [20, 21], or in a mechanical system characterized by an oscillator with a ferromagnetic

iron mass in an external magnetic field [22].

A special case of “complex” hysteresis is given by an elementary play or backlash operator, which also appears in various dynamical systems [23, 24]. In the same manner as the PM is defined by a superposition of elementary relay blocks, the so called Prandtl-Ishlinskii model for “complex” hysteresis is build of elementary play operators [25]. There are various works on dynamical systems with this type of hysteresis, mainly in the context of control theory [26, 27].

Another prominent model, which shows “complex” hysteresis is the Random Field Ising Model (RFIM) at zero temperature. It can be used, for example, to model magnetic dipole moments of atoms. Originally the RFIM was introduced to study phase transitions with a renormalization group approach [28]. Later, also the hysteretic features of the RFIM gained some interest [9, 29–31].

In [32] we studied a degenerated case of a RFIM without hysteresis, where nearest neighbor interactions were neglected. In this paper, as an extension of [32], we consider an ensemble of independent spin pairs, which we will call “dimers”. We analyse the system dynamics of such a gas of dimers at zero temperature and show, that hysteresis is possible. In this case always two spins form an elementary hysteresis loop or relay and we show that this kind of hysteresis can be equivalently modeled by a PM. Already for a single dimer, we can find chaotic solutions and bifurcations, which are typical in piecewise-smooth systems. We calculate the fractal dimensions of several chaotic attractors and compare the results of the many spin systems with the thermodynamical limit. This sheds some light on how the thermodynamic limit is approached by the piecewise-smooth system. We also determine the self-averaging properties of the fractal dimensions of the chaotic attractors.

The organization of the paper is as follows. In Sec. II

we introduce the model and the different types of spin-spin interactions. Sec. III is about the methods, which are necessary for the analysis of the dynamical system with hysteresis. In particular, we describe specific methods for handling the discontinuities in piecewise-smooth systems, we derive a relationship between the spin dimers and the PM, which is used to describe the system dynamics in the thermodynamical limit, and some remarks on the numerics and the calculation of the Lyapunov exponents are given. In Sec. IV the results are presented, at first for the single dimer dynamics and later for many dimers, followed by a conclusion in Sec. V.

II. MODEL

We study a periodically driven damped harmonic oscillator, which gets feedback from an ensemble of independent spin dimers at zero temperature. On the one hand, the driven harmonic oscillator is a classical and well-studied linear dynamical system. On the other, the spin dimers act as a model for complex hysteresis. In this section we briefly describe the two building blocks of the system and the coupling to each other. A more detailed derivation can be found in [32].

A. Oscillator model

We consider the motion of a magnetizable point mass (which we call “iron” for simplicity) in an external magnetic field. The position q of the iron mass is determined by the dynamics of a periodically driven harmonic oscillator in this field. In general the magnetization M of the iron mass in dependency of the magnetic field B is determined by the orientation of the intrinsic magnetic domains, which can be modeled e. g. by a RFIM. Here, as a simplification we want to consider the magnetic system as an ensemble of independent spin dimers (a spin gas at zero temperature), also we assume a constant magnetic field gradient $B(q) \sim q$, such that the magnetization M changes with the position $q(t)$ of the oscillator (cf. [22]).

In dimensionless variables the equation of motion can be written as

$$\ddot{q}(t) + 2\zeta\dot{q}(t) + q(t) = \cos \Omega t + F_{\text{hys}}(t), \quad (1)$$

where $q(t)$ denotes the position of the oscillator at time t , ζ is the damping ratio of the system, and Ω is the scaled excitation frequency. The mass of the oscillator is normalized to one and time t is rescaled such that the eigenfrequency of the oscillator is equal to one. The hysteresis force $F_{\text{hys}}(t)$ is the force due to the magnetization of the of the iron mass, which is determined by the spin dimers, the local random fields and the external magnetic field, which changes linearly with the oscillator position q . Here, we assume that the hysteresis force depends linearly on the magnetization, i. e., $F_{\text{hys}}(t) = CM[q](t)$,

where C is the coupling constant and $M[q](t)$ denotes a functional that can depend on the whole trajectory of $q(t')$ up to time t . This is due to the fact, that in contrast to [32] here the spin-spin interactions are not neglected, thus there is more than one metastable state, which the spin system can reach. Hence hysteresis is possible as described in Sec. II B and Sec. II C. Introducing the state variable $\mathbf{x} = (q, v = \dot{q}, \phi = \Omega t)^T$ in general, the oscillator dynamics can be described by

$$\dot{\mathbf{x}}(t) = \begin{pmatrix} v(t) \\ -2\zeta v(t) - q(t) + \cos \phi(t) + CM[q](t) \\ \Omega \end{pmatrix}, \quad (2)$$

where the ensemble of spin dimers is used to update the magnetization M after each variation of $q(t)$.

B. Independent spin dimers at zero temperature

As mentioned before the spin system of the iron mass is modeled by an ensemble of independent spin dimers. Thus for an even number of N spins, we have $N/2$ spin dimers. A spin dimer is given by the two spins σ_i and σ_{i-1} with even $i = 2, 4, 6, \dots, N$, and as usual the magnetization per spin is given by the mean over all spins $M = \frac{1}{N} \sum_{i=1}^N \sigma_i$. Nearest neighbor interactions, with the coupling strength J , only occur between the two spins of one spin dimer. So this system is not a spatially extended system. Also the state $\sigma_i \in \{-1, +1\}$ of each spin is affected by the local field b_i and an external magnetic field proportional to q , so in dimensionless variables the Hamiltonian can be written as:

$$H = \sum_{k=1}^{N/2} \left[-J\sigma_{2k-1}\sigma_{2k} - \left(\sigma_{2k-1}(q+b_{2k-1}) + \sigma_{2k}(q+b_{2k}) \right) \right]. \quad (3)$$

Since in this paper we deal with spin dimers at zero temperature, the internal spin dynamics of the system is totally deterministic and can be described by the usual single spin flip dynamics [33, 34]. This means a metastable state at time t is given, if each spin points in the direction of its local field $F_i(t)$, that is

$$\sigma_i(t) = \text{sgn}(F_i(t)), \quad \forall i = 1, 2, 3, \dots, N \quad (4)$$

$$\text{with } F_i(t) = \begin{cases} J\sigma_{i-1}(t) + q(t) + b_i, & i \text{ even} \\ J\sigma_{i+1}(t) + q(t) + b_i, & i \text{ odd} \end{cases}. \quad (5)$$

Eq. (4) is often called metastability condition. Here the spin system is first updated until a metastable state is reached and after that the oscillator position q can change according to the new magnetization M (see Sec. III D). This property can be characterized as adiabatic limit [35].

C. Two pairwise interacting spins

We start by discussing the special case of $N = 2$ spins coupled to each other, i.e. with one spin dimer. In this case the metastability condition from Eq. (4) reads

$$\sigma_{1/2} = \text{sgn}(J\sigma_{2/1} + q + b_{1/2}), \quad (6)$$

where $\sigma_{1/2}$ denotes either the “first” or the “second” spin of each spin dimer. Without loss of generality we assume $b_1 > b_2$. Then, from $2^N = 4$ (not necessarily metastable) internal states, only three metastable states remain. The conditions to find the two spins in one of the three states can be derived from Eq. (6). They are summarized in Table I and illustrated in Fig. 1. We can see, that qualitatively three different scenarios under a variation of the position q are possible. The first scenario occurs for

$\downarrow\downarrow$	$q < J - b_1$
$\downarrow\uparrow$	not possible
$\uparrow\downarrow$	$J - b_1 < q < -J - b_2$
$\uparrow\uparrow$	$-J - b_2 < q$

TABLE I. Possible metastable states and corresponding conditions for two coupled spins with $J > 0$. Since we assume $b_1 > b_2$, the second configuration is not a metastable state. The third configuration is only possible, if $J - b_1 < -J - b_2$, i.e. for $2J < b_1 - b_2$.

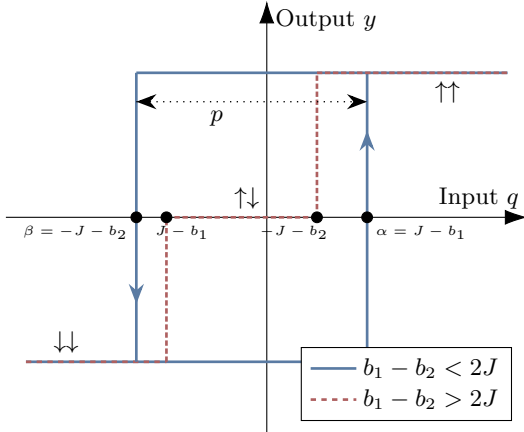


FIG. 1. Graphical illustration of the magnetization (output y) of a spin dimer with $J > 0$ and $b_1 > b_2$. For $2J > b_1 - b_2$ the system shows elementary hysteresis and therefore memory. In contrast, for $2J < b_1 - b_2$ a different scenario occurs. Starting with both spins down and increasing the input q , at first one spin flips upward at $q = J - b_1$ and later at $q = -J - b_2$ the second spin flips upward.

$b_1 - b_2 > 2J$. In this case, for $q < J - b_1$ the two spins are pointing downwards ($\sigma_1 = \sigma_2 = -1$). By increasing q , the first spin σ_1 flips up at $q = J - b_1$ and the second spin σ_2 flips at $q = -J - b_2$ (red dashed line in Fig. 1). In the second scenario, for $b_1 - b_2 = 2J$, only one jump at $q = J - b_1 = -J - b_2$ occurs, where both spins flip at the same position. In the third scenario for $b_1 - b_2 < 2J$, both

spins pointing downwards for $q < -J - b_2$. By increasing q , both spins flip upward at $q = \alpha = J - b_1$. However, starting at $q > J - b_1$, where both spins are in the upper state, and decreasing q , both spins flip downward at $q = \beta = -J - b_2$ with $\beta < \alpha$ (blue solid curve in Fig. 1). Hence, in this case, for $\beta < q < \alpha$ two metastable states exist, where β and α are the lower and higher jump value, respectively. This means that in scenario three an elementary hysteresis loop occurs for two interacting spins, and the internal state depends on the history of q , or in other words, the system shows memory.

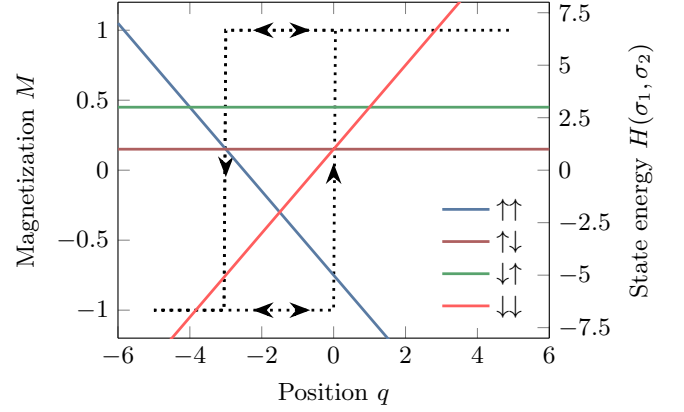


FIG. 2. Numerical validation of the behavior of two spins with the coupling constant $J = 2$ and the local fields $b_1 = 2$, $b_2 = 1$. The colored lines show the energies $H(\sigma_1, \sigma_2)$ of the different internal states of the system. It can be seen, that for a single spin flip dynamics only three states of the system can be reached ($\uparrow\downarrow$, $\downarrow\downarrow$, $\uparrow\uparrow$), whereas one state is impossible to reach ($\downarrow\uparrow$). Also the related threshold values $\beta = -3$ and $\alpha = 0$ are given by the change of the energetically favorable states, indicated by the corresponding intersection points.

A numerical example with $J = 2$, $b_1 = 2$ and $b_2 = 1$ is presented in Fig. 2. One can see the output, the magnetization M (dotted black line) depending on its input q . Indeed, the first spin flips upward at $q = J - b_1 = 0$, and the second spin flips downward at $q = -J - b_2 = -3$, which are the boundaries α and β of the elementary hysteresis loop, respectively. Thus, the width p of the loop is equal to $p = 2J - b_1 + b_2 = 3$. In addition, we have plotted the energy $H(\sigma_1, \sigma_2)$ of the four spin configurations $\{\sigma_1, \sigma_2\}$, $\sigma_i = \pm 1$ as functions of q , which can explain the spin flips from an energetic point of view. For $q < \beta = -3$ all spins are pointing down $\downarrow\downarrow$, which is the state with the lowest energy ($\downarrow\downarrow$). By increasing q , the energy level of the downward state increases, and at $q = -1.5$, the $\uparrow\uparrow$ -state becomes the state with the lowest energy ($\uparrow\uparrow$). However, this state cannot be reached by a single spin flip (cf. Sec. II B), and therefore, the system stays in the metastable state $\downarrow\downarrow$. Later, at $q = \alpha = 0$ the $\uparrow\downarrow$ -state ($\uparrow\downarrow$) has the same energy as the $\downarrow\downarrow$ -state, as a consequence, the first spin flips, and the resulting state is $\uparrow\downarrow$. However, this state is not metastable because a second single spin flip is possible, for which the system can

reach the energetically favorable $\uparrow\uparrow$ -state. Since the spin system is only updated if a metastable state is reached, at $q = \alpha = 0$ the system immediately jumps from $\downarrow\downarrow$ to $\uparrow\uparrow$. A similar procedure occurs for decreasing values of q , where the reverse jump occurs at $q = \beta = -3$. From this energetic picture it is also clear, that only three of the four possible states can be reached, because the $\downarrow\uparrow$ -state has always a larger energy than the $\uparrow\downarrow$ -state. These results are fully consistent with the results in Table I.

D. Many spin dimers

In this paper we study the special case of spin dimers, where each of the dimers has the same width of the hysteresis loop, therefore without loss of generality and consistent with the case of a single spin dimer, we assume $b_{i-1} > b_i$, with $i = 2, 4, \dots, N$. Now we choose the two local field values b_i and b_{i-1} such that an elementary hysteresis loop is formed and that each loop has the same width ($p = 2J - b_{i-1} + b_i > 0$). Since by definition $b_{i-1} > b_i$, we obtain $0 < p < 2J$ for possible fixed widths p of the elementary hysteresis loops. The lower and the higher jump values are given by $\alpha_k = J - b_{2k-1}$ and $\beta_k = -J - b_{2k}$, respectively, where $k = 1, \dots, N/2$ numbers the spin dimers.

This paper deals, on one hand, with spins in a random field. On the other hand the hysteresis loops associated with the spin dimers should all have the same width p . Therefore, if one local field value, for example b_{i-1} , is chosen randomly, the other field value b_i is automatically determined by $b_i = p - 2J + b_{i-1}$. Correspondingly the jump values are given by

$$\alpha_k = J - b_{2k-1} \quad (7)$$

$$\beta_k = J - b_{2k-1} - p. \quad (8)$$

For practical reasons instead of choosing one of the field values b_{i-1} or b_i for each dimer, we will choose the center $s_k = (\alpha_k + \beta_k)/2$ of each elementary hysteresis loop to be Gaussian distributed and uncorrelated with $\overline{s_k s_l} = R^2 \delta_{kl}$, $\overline{s_i} = 0$ and determine the related values as $b_{2k-1} = -s_k + J - \frac{p}{2}$ and $b_{2k} = -s_k - J + \frac{p}{2}$. Here \overline{X} denotes the average of X over all realizations of the quenched disorder field $\{b_i\}$.

III. METHOD

A. Preisach Model

The harmonic oscillator coupled to pairwise interacting Ising spins results in a system with $N/2$ superposed elementary hysteresis loops, which resembles the definition of the PM. Thus we want to give a quick overview of the basic ideas of the PM. The building blocks of the PM [17, 18] are the elementary hysteresis loops, which are also called Preisach units, hysterons or relays. An

example of such an elementary hysteresis loop is given by the blue solid curve (—) in Fig. 1. For a given input $q(t)$ the output $y_{\alpha\beta}[q](t)$ of a Preisach unit at time t with threshold values α and β ($\alpha > \beta$) is given by

$$y_{\alpha\beta}[q](t) = \begin{cases} +1 & \text{for } q(t_0) \geq \alpha \text{ and } q(t_1) \geq \beta, \forall t_1 \in [t_0, t], \\ -1 & \text{for } q(t_0) < \beta \text{ and } q(t_1) < \alpha, \forall t_1 \in [t_0, t], \end{cases} \quad (9)$$

where t_0 specifies the last time at which the input was outside the bistable interval $[\beta, \alpha]$. Since, the time t_0 depends on the behavior of the position function $q(t')$ with $t' < t$, the output $y_{\alpha\beta}[q](t)$ of the Preisach units is, in general, a functional. The output of the whole PM is a superposition of the output of infinitely many Preisach units with different threshold values weighted by the so-called Preisach density $\mu(\alpha, \beta)$. For our ferromagnetic interpretation of the complex hysteresis, the output of the PM is the magnetisation $M[q](t)$, which is defined as

$$M[q](t) = \iint_{\alpha \geq \beta} \mu(\alpha, \beta) y_{\alpha\beta}[q](t) d\alpha d\beta. \quad (10)$$

The parameters α and β span a surface, the so-called Preisach plane, which can be used to illustrate the Preisach density or the internal state of the PM. However, since $\alpha > \beta$ only a half-plane in the two-dimensional Preisach plane is relevant. A very common transformation of the Preisach plane is a rotation by $+\pi/4$ and a scaling by a factor $1/\sqrt{2}$, where the new variables s and r are specified by

$$s = \frac{\alpha + \beta}{2}, \quad r = \frac{\alpha - \beta}{2}. \quad (11)$$

The variable s describes the center and r is the half of the width of an elementary hysteresis loop ($r > 0$).

In the new coordinates the relationship between the PM and the ensemble of spin dimers becomes clear, by identifying corresponding elementary hysteresis loops from each system: the values α_k and β_k from Eq. (8) in Sec. IID are identical to the threshold values captured by the Preisach density of Eq. (10). For a finite ensemble of spin dimers the Preisach density is given by the discrete density $\mu(\alpha, \beta) = \sum_k^{N/2} \delta(\alpha - \alpha_k) \delta(\beta - \beta_k)$, whereas a continuous Preisach density $\mu(\alpha, \beta)$ corresponds to the thermodynamic limit of the spin system. For instance, if we consider the example from Sec. IID, where we assumed that the center s of the elementary hysteresis loops is Gaussian distributed with $s \sim \mathcal{N}(0, R^2)$ and the width of the each loop is fixed equal to p , the corresponding transformed Preisach density $\tilde{\mu}(r, s)$ given as

$$\tilde{\mu}(r, s) = \mu(s) \delta(r - \frac{p}{2}), \quad (12)$$

with

$$\mu(s) = \frac{1}{\sqrt{2\pi R^2}} e^{-\frac{s^2}{2R^2}}. \quad (13)$$

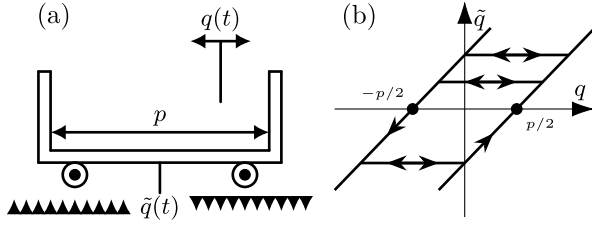


FIG. 3. (a): Illustration of mechanical play by using the analogue of a wagon. The input $q(t)$ is given by e. g. a finger, which moves the wagon. If the finger touches the right or the left side of the wagon, respectively, the output is given by $\tilde{q}(t) = q(t) + p/2$ and $\tilde{q}(t) = q(t) - p/2$, whereas the output stays constant if the finger moves in between both sides of the wagon. The black arrows on the left and right side of \tilde{q} illustrate the separation of the spin dimers (ordered according to the center values of their associated hysteresis loops) in the down or up state, respectively. (b): Representation of the movement of the wagon in the input-output-plane.

This relationship between the system with pairwise interacting spins and the Preisach model is especially helpful for calculating the magnetization if the number of spin dimers goes to infinity.

B. Play Operator and Thermodynamic limit

From Eq. (12) one can see, that the width of the elementary hysteresis loops are delta distributed and the center is Gaussian distributed in the Preisach plane. It has been shown, that when using a uniformly distributed center of the loops, the output of the PM is given by the so called “play” or “backlash” operator [36, 37]. The output $\tilde{q}(t)$ of this operator at time t is given by:

$$\tilde{q}(t) = \max\left\{q(t) - \frac{p}{2}, \min\left\{q(t) + \frac{p}{2}, \tilde{q}(t_i)\right\}\right\}, \quad (14)$$

where $t_i < t$ is the time when the last extremum of the input q was attained.

Since t_i depends on the history of the input, $\tilde{q}(t)$ is a functional of the input function $q(t')$ with $t' < t$. The expression in Eq. (14) can be visualized by using a mechanical analogue consisting of a wagon controlled by a finger movement (see Fig. 3(a)). Here the input $q(t)$ is the position of a finger that moves a wagon. The center $\tilde{q}(t)$ of the wagon only changes, if the finger position during a movement is identical with the right ($\tilde{q}(t) = q(t) - \frac{p}{2}$) or the left position ($\tilde{q}(t) = q(t) + \frac{p}{2}$) of the wagon, respectively. In case the finger stands in between both walls, $\tilde{q}(t)$ does not change and is identical to its last position in a movement. The corresponding behavior in the input-output-plane is illustrated in Fig. 3(b).

Because each spin dimer in our system contributes one elementary hysteresis loop, we can make a connection between the mechanical play and the system of spin dimers: The input $q(t)$ corresponds to the position of the

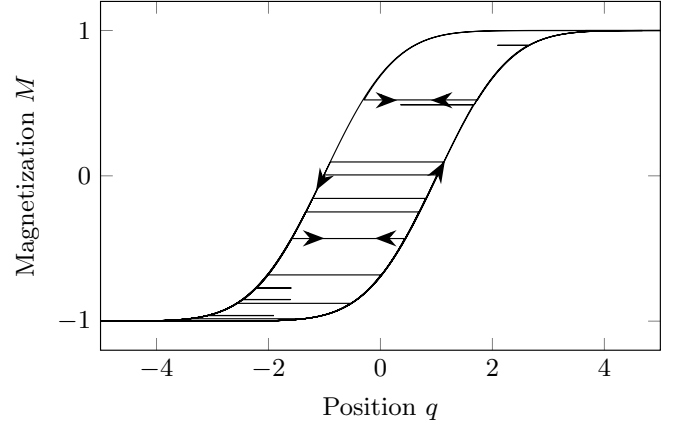


FIG. 4. Illustration of the output of the spin dimer system in its thermodynamic limit, resulting in an operator in form of a modified mechanical play ($p = 2$, $R = 1$) given by Eq. (16). The input-output behavior is characterized by a major loop formed by the functions f_- and f_+ from Eqs. (17), (18) and degenerate inner loops.

finger in the mechanical play and to the value of the external field in the spin system. Now one imagines the dimers placed on the q -axis according to their center values s_k (see IID), i. e. in creasing order from left to right (the arrows in Fig. 3(a)). Then a movement of the wagon (with center position at $\tilde{q}(t)$) to the right (left) corresponds to an increasing (decreasing) field, which flips dimer states centered at position $\tilde{q}(t) = q(t) - p/2$ from -1 to $+1$ ($\tilde{q}(t) = q(t) + p/2$ from $+1$ to -1). If the finger moves inside the wagon without touching the walls the position \tilde{q} of the wagon stays at its last position of a movement. This corresponds to a variation of the external field within the elementary hysteresis loop which switched at last. Thus the position \tilde{q} of the wagon separates the dimers in the down-state from the dimers in the up-state. For this to hold we assume, that initially all dimers were in the down-state and the external field assumed its minimal value. In Fig. 3 we illustrated this by the arrows pointing down on the left side of \tilde{q} and pointing up on the right side, respectively. Hence the magnetization in the thermodynamical limit can be calculated by summing over all dimer states or, in the thermodynamic limit by an integration over the density of the centers of the elementary hysteresis loops, given by $\mu(s)$ from Eq. (13):

$$M[q](t) = 2 \int_{-\infty}^{\tilde{q}(t)} \mu(s) ds - 1 = \operatorname{erf}\left(\frac{\tilde{q}(t)}{\sqrt{2}R}\right), \quad (15)$$

where $\tilde{q}(t)$ is given by Eq. (14). Using the monotonicity of the error function this can also be written in a more compact way:

$$M[q](t) = \max\left\{f_+(q(t)), \min\left\{f_-(q(t)), M[q](t_i)\right\}\right\}, \quad (16)$$

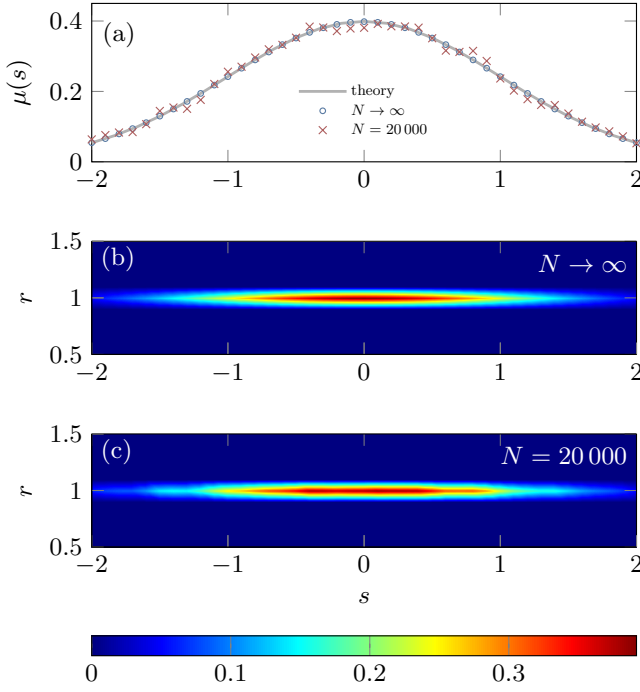


FIG. 5. (a): Comparison of the numerically calculated and theoretical density $\mu(s)$ from Eq. (13). (b), (c): The numerically determined Preisach density plotted in the r - s -plane. $N \rightarrow \infty$ denotes the system in its thermodynamic limit and $N = 20\,000$ denotes the piecewise-smooth system. The randomness and the width of each elementary hysteresis loop are set to $R = 1$ and $p = 2$.

with

$$f_{-}(q(t)) = \operatorname{erf}\left(\frac{q(t) + \frac{p}{2}}{\sqrt{2}R}\right), \quad (17)$$

$$f_{+}(q(t)) = \operatorname{erf}\left(\frac{q(t) - \frac{p}{2}}{\sqrt{2}R}\right). \quad (18)$$

In Fig. 4 an illustrative case with $p = 2$ and $R = 1$ is shown. Note, that Eq. (16) can also be derived by integrating Eq. (10) with a Preisach density $\mu(\alpha, \beta)$ obtained from Eqs. (12) and (13) using the transformation from Eq. (11).

As a verification of our calculations we determined the Preisach density $\mu(r, s)$ of the piecewise-smooth system for $N = 20\,000$ spin dimers with randomness $R = 1$, as well as for the system in its thermodynamic limit, given by Eq. (16). A detailed description how to determine $\mu(r, s)$ in an experimental way by scanning the whole Preisach plane gradually can be found in [8, 18]. The results are shown in Fig. 5. We find, that for both systems the density coincides within numerical accuracy with the result from Eqs. (12) and (13).

Lyapunov exponents.—To determine the full Lyapunov spectrum of a dynamical system given by Eq. (2) with a Preisach nonlinearity (10), we developed a method, which will be presented in a future paper.

C. Piecewise-smooth system

It is totally clear, that the spin system contains continuous degrees of freedom of the harmonic oscillator as well as discrete degrees of freedom of the spins, and therefore, it can be treated by methods from piecewise-smooth system theory [38]. The investigation of such systems mainly can be found in the field of relay feedback systems [39], gear dynamics [40] or systems with dry friction [41], but also in the field of tapping-mode atomic force microscopy [42]. Here, we briefly introduce the theory of piecewise-smooth dynamical system, that we have used to analyze our system. More details can be found in [32].

In a system with an even number of N spins, we have $N/2$ spin dimers and both two spins in one dimer only can be in the down state or in the up state. This gives us a phase space $\{q, v, \Omega t \bmod 2\pi\} \times \{\pm 1\}^{N/2}$. In the following we call the discrete spin states *sheets* S_n with $n = 1, \dots, 2^{N/2}$ and the transition point from on sheet S_i to another S_j is called q_{ij}^* . Since different S_n are related to the same magnetization, there are $k = 0, \dots, N/2$ different values for the magnetization $M_n = \frac{4k}{N} - 1$. Hence Eq. (2) becomes

$$\dot{\mathbf{x}}(t) = \begin{pmatrix} v(t) \\ -2\zeta v(t) - q(t) + \cos \phi(t) + CM_k \end{pmatrix}. \quad (19)$$

We will discuss this in more detail by looking at the example of $N = 4$ spins corresponding to two spin dimers. In Fig. 6 a schematic trajectory of the full phase space is shown. In the case of two spin dimers, there are 4 different sheets S_1, \dots, S_4 . Each sheet corresponds to one spin dimer configuration illustrated by the two boxes with arrows. The related values of the magnetization are also illustrated by $M_0 = -1$ (S_1), $M_1 = 0$ (S_2, S_3) and $M_2 = +1$ (S_4). Also for two spin dimers there are four threshold values, where a spin dimer flips. Here we will assume without loss of generality, that the upper threshold value $\alpha_1 = q_{12}^*$ of the left (“first”) spin dimer in Fig. 6 is lower than the upper value of the right (“second”) dimer $\alpha_1 < \alpha_2 = q_{23}^*$. Imagine an arbitrary trajectory starting at \mathbf{x}_0 in sheet S_1 . If the position q is greater than the upper threshold value of the first dimer $\alpha_1 = q_{12}^*$, the first dimer flips from its down to the up state and the trajectory evolves within the sheet S_2 . Again, if q becomes greater than $\alpha_2 = q_{23}^*$ the second dimer flips up and the system stays in S_3 . Because of the same width of the hysteresis of each dimer we have $\beta_1 = q_{21}^* < \beta_2 = q_{32}^*$, hence if q becomes lower than the threshold $\beta_2 = q_{32}^*$ the same second dimer changes its orientation again. The trajectory evolves again in S_2 . Finally if $q < \beta_1 = q_{21}^*$ the first dimer flips back to the down state and the system reached S_1 .

Note, that because of $p = \text{const.}$ for each spin dimer, the inner $2^{N/2}$ states reduces to $N/2 + 1$ states corresponding to one unique value M_n . Therefore the system shows local memory. This also can be seen in the case of the thermodynamic limit (see Sec. IIIB), where for

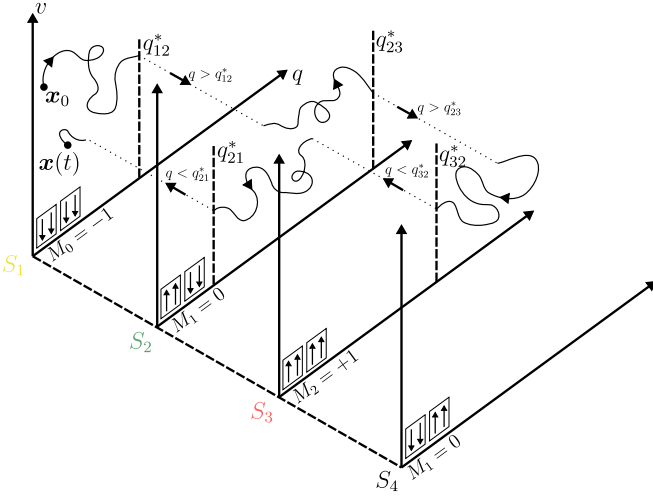


FIG. 6. Schematic trajectory evolving in the phase space given by $\{q, v, \Omega t \bmod 2\pi\} \times \{\pm 1\}^{N/2}$. The discret values of the spin dimer configurations are illustrated by different sheets S_1, \dots, S_4 . The full description is given in the text.

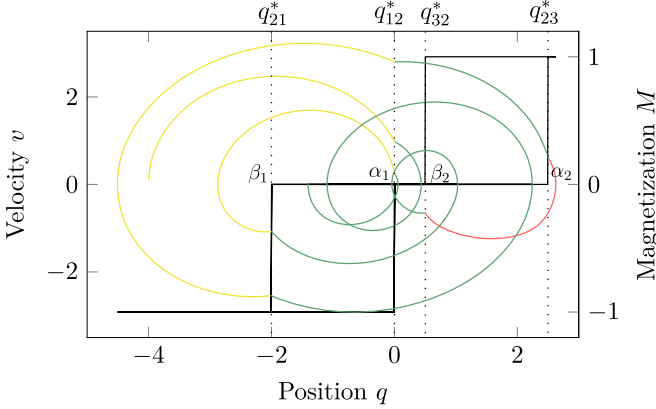


FIG. 7. Simulation of an actual trajectory with $J = 2$, $p = 2$, $b_1 = 2$, $b_2 = 0$, $b_3 = -0.5$ and $b_4 = -2.5$. The different sheets of the phase space are illustrated by different colors: $\text{yellow} \hat{=} S_1$, $\text{green} \hat{=} S_2$, $\text{red} \hat{=} S_3$.

a given point (q, M) the slope of the hysteresis curve is unique [43]. This behavior is also reflected by the fact, that in case of the play operator only one return-point contribute to the memory of the system.

In Fig. 7 we also simulated an actual trajectory and color coded the different sheets by different colors ($\text{yellow} \hat{=} S_1$, $\text{green} \hat{=} S_2$, $\text{red} \hat{=} S_3$). Here the following parameters were chosen: $J = 2$, $p = 2$, $b_1 = 2$, $b_2 = 0$, $b_3 = -0.5$ and $b_4 = -2.5$. For the threshold values we find in accordance with the simulation $\alpha_1 = 0$, $\beta_1 = -2$, $\alpha_2 = 2.5$ and $\beta_2 = 0.5$.

Lyapunov exponents.—Now we want to describe the calculation of the Lyapunov exponents for a system like Eq. (19), which specifies the average exponential behavior of an infinitesimal perturbation of a reference trajectory. From Eq. (19) we can see, that our system behaves

regular within the smooth regions S_k of the phase space. In this case the system is a damped harmonic oscillator with periodic driving force and an additional constant hysteresis force $F_{\text{hys}} = CM_k$. The corresponding Lyapunov spectrum is given by $\lambda_1 = 0$, $\lambda_2 = -\zeta$, $\lambda_3 = -\zeta$. Hence, chaotic behavior can only be introduced by the intersection of the trajectories with a boundary between two smooth regions. This means, that specific attention must be paid for the calculation of the Lyapunov exponents at these intersections.

The whole concept for the description of chaotic behavior in systems with discontinuities is called Discontinuity Mapping (DM) [44–47]. The basic idea is the calculation of a correction map \mathbf{Q} , which characterizes the intersection with a boundary for a point very close to a discontinuity in the phase space. The idea behind the DM is as follows. In general, the reference trajectory and the perturbed trajectory does not reach the intersection point at the same time. However, for the calculation of the Lyapunov exponents with infinitesimal perturbations it is required to apply the discontinuity mapping for the reference and the perturbed trajectory at the same time. For our system the DM can be defined as

$$\mathbf{x} \rightarrow \mathbf{Q}(\mathbf{x}) = \begin{pmatrix} q \\ C(\Delta M)\delta t + v \\ \phi \end{pmatrix}, \quad (20)$$

where $\delta t = \frac{q^* - q}{v^*}$. Here q^* is the intersection point with the boundary, v^* is the velocity at intersection and ΔM is the change of the magnetization from one boundary to the other.

Then, for infinitely small perturbations $\delta \mathbf{x}$ the Jacobian $\mathbf{X} = \partial_{\mathbf{x}} \mathbf{Q}(\mathbf{x})$ of the map $\mathbf{Q}(\mathbf{x})$ can be used to calculate the perturbation $\delta \mathbf{x}^+(t^*)$ after intersecting the discontinuity boundary $\delta \mathbf{x}^+(t^*) = \mathbf{X} \delta \mathbf{x}^-(t^*)$ from the perturbation directly before the boundary crossing $\mathbf{x}^-(t^*)$. The matrix \mathbf{X} is often called saltation matrix. For our system we find

$$\mathbf{X} = \begin{pmatrix} 1 & 0 & 0 \\ \frac{1}{v^*} C \Delta M & 1 & 0 \\ 0 & 0 & 1 \end{pmatrix}. \quad (21)$$

With the saltation matrix \mathbf{X} , the largest Lyapunov exponent for a reference trajectory with only one crossing at time t^* can be written as

$$\lambda = \lim_{t \rightarrow \infty} \frac{1}{t} \ln \frac{|\mathbf{Y}(t, t^*) \mathbf{X} \mathbf{Y}(t^*, 0) \delta \mathbf{x}_0|}{|\delta \mathbf{x}_0|}, \quad (22)$$

where $\mathbf{Y}(t, t')$ is the fundamental solution of the variational equation $\delta \dot{\mathbf{x}}(t) = \mathbf{D} \delta \mathbf{x}(t)$ of the Ordinary Differential Equation (ODE) (19) from time t' to t and \mathbf{D} denotes the Jacobian matrix. In general, at each crossing a multiplication with the corresponding saltation matrix is necessary and we use a QR-decomposition to calculate the Lyapunov exponents for large t . A more detailed description can be found in [32].

To use the concept of DM for a complex hybrid phase space described in Sec. III C it is useful to consider the system in a different way. Therefore we will treat the system like it is evolving in the continuous phase space $\{q, v, \Omega t \bmod 2\pi\}$, so that the Lyapunov exponents are well defined. This phase space consist of the smooth regions S_i , which are separated by the boundaries q_{ij}^* . But in contrast to the case of independent spins, which we investigated in [32], here to positions of the boundaries change over time. Thus some of the boundaries are “active” or “inactive” over time. In the next section we will describe how to use this point of view to simulate trajectories of this piecewise-smooth system.

D. Numerics

Since the disorder values b_i are quenched and the spins are pairwise coupled to each other, we are able to calculate a priori the solution $x(t)$ at all possible discontinuities, where a spin flips can occur. For the generation of a trajectory of the piecewise-smooth system we start with an initial condition at $t = 0$ with the corresponding initial magnetization M_k and use the analytical solution of the linear system (19), which is described in [32]. By discretizing this solution with time step Δt we propagate the trajectory until the first spin flip occurs, where the magnetization jumps from the initial value M_k to some other value. At all potential spin flips we determine the metastable state of the spin dimer system to check whether this boundary is an “active” boundary, i. e., whether a spin flip occurs or not. This depends on the history of the system. If it is indeed an intersection point with a jump of the magnetization we use a root finder to exactly determine the time of the discontinuity. After the boundary we can simply use the analytic solution with the new magnetization value to propagate the trajectory within the next smooth region of the phase space.

In case of a large number of spins the sizes of the smooth regions in the phase space are very small and the algorithm based on the analytical solution becomes very slow. For increasing the speed of the algorithm in this case we use a linearization of the solution to calculate directly the time to the next boundary, therefore in this case no root finder is necessary.

IV. RESULTS

Here we present numerical results on the dynamic behavior of the periodically driven harmonic oscillator. If not stated otherwise, for the numerical simulations we used the initial conditions and model parameters from Table II.

Parameter	Symbol	Value
damping ratio	ζ	0.05
excitation frequency	Ω	1.0
initial position	q_0	-1.0
initial velocity	v_0	0.1
initial spin orientation	$\sigma_i(t=0)$	-1
spin coupling strength	J	2.0
randomness	R	1.0
elementary hysteresis loop width	p	2.0

TABLE II. Model parameters and initial conditions of the numerical simulations.

A. Bifurcations and attractors

Two spins.—At first, we study the basic system with a single dimer ($N = 4$). In this case we numerically determine the Poincaré section for $q(\phi = 0)$ and the corresponding largest Lyapunov exponent λ_{\max} in dependency on the coupling strength of the magnetization C . The disorder realization is given by $b_1 = 1$, $b_2 = -1$. The related bifurcation diagram is shown in Fig. 8. Starting with a large C and decreasing C step by step one finds, that at $C = 9$ the system undergoes a period-adding cascade (—). This is in accordance with the theoretic value of C , which can be calculated by using the results from [32]. In the bifurcation diagram we can also find period-adding scenarios with chaotic regimes in between (—) and an immediate jump to chaos (—). These are typical scenarios for piecewise-smooth systems with grazing behavior and piecewise-smooth square-root maps [48–50]. In [32] we derived the Poincaré-section discontinuity mapping and the zero-time discontinuity mapping for the system with a single spin, which indeed showed these kind of maps. Therefore it can be seen, that the system with only one spin and with two coupled spins behave in a similar way. It is worth to emphasize, that when changing the initial condition and/or the disorder realization the qualitative behavior of the bifurcations stays the same, but the position of the periodic windows and the chaotic regimes may change.

For only a few number of spins the overall behavior of the piecewise-smooth system does not change much in comparison to the system with only two spins. An interesting questions arises, if the number of spins becomes very large ($N \rightarrow \infty$). From Eq. (21) we can see that, on the one hand, the number of boundaries increases for an increasing number of spins, but, on the other hand, the influence of each boundary becomes smaller because $\mathbf{X} \rightarrow \mathbf{I}$. In this case, the hysteresis force F_{hys} becomes smoother, depends nonlinearly on the oscillator position $q(t)$, and chaos is still possible [32].

Many spins.—A comparison between the system in its thermodynamic limit ($N = \infty$) and the piecewise-smooth system for $N = 20\,000$ spins is illustrated in Fig. 10, where the same parameters and initial conditions are used for both systems. It seems, that the trajectory, the Poincaré section and the magnetization curve behave in

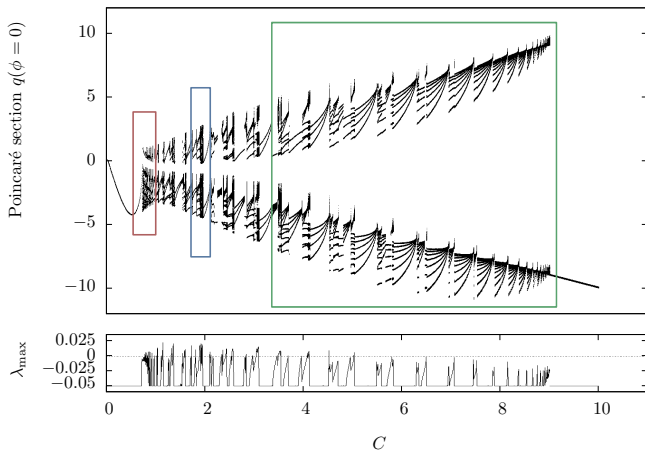


FIG. 8. For two coupled spins $N = 2$ the system shows the bifurcation scenarios expected from piecewise-smooth square-root maps, illustrated by the different colored boxes: immediate jump to robust chaos with a positive largest Lyapunov exponent λ_{\max} (—), period-adding with chaotic windows (—) and overlapping period-adding cascade (—). The local disorder fields are $b_1 = 1$ and $b_2 = -1$.

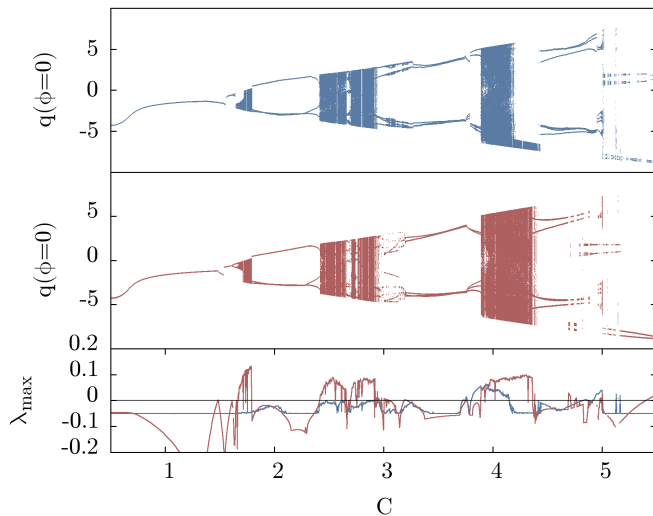


FIG. 9. The bifurcation diagrams with the largest Lyapunov exponent for the piecewise-smooth system with a large number of spins $N = 20\,000$ (■) does not show the typical bifurcation scenario, which is known from piecewise-smooth systems with grazing behavior. Instead, the behavior is very similar to the behavior of the continuous system (■) in the thermodynamic limit ($N = \infty$).

a similar way, and there could be a similarity between the fractal dimension of the chaotic attractor of the discrete and the continuous systems. We also determined the bifurcation diagram for both systems, which can be seen in Fig. 9. First of all, we find that the typical bifurcation scenarios for piecewise-smooth systems, as was found in the system with only a few number of spins, vanish. This is an indicator, that only transversal intersections of the trajectory with the boundaries are important for systems

with a large number of spins, compared to tangential intersections (grazing). This is similar to the behavior we found in the system for independent spins [32]. In general, the two bifurcation diagrams are quite similar, but they differ within the periodic windows. This is due to the fact, that we only used one initial condition and always the same disorder realization for determining the Poincaré section. Like in the case of only one spin dimer, the exact position of the chaotic and periodic windows can change when changing these values. Another remarking point is that the calculated largest Lyapunov exponent λ_{\max} of the piecewise-smooth system differs from λ_{\max} of the system in its thermodynamic limit. For example, in the Poincaré section one can find two chaotic windows near $C \in [1.7, 1.8]$ and $C \in [2.5, 3.0]$, where the largest Lyapunov exponent λ_{\max} is negative.

B. Fractal dimension of the chaotic attractor

For a quantitative measure of the similarity between the chaotic attractor of the piecewise-smooth system with a large but finite number of spins and the continuous system in the thermodynamic limit, we analyze the box counting D_{BC} and the Kaplan-Yorke dimension D_{KY} of the chaotic attractors of both systems [51, 52]. We focus on two examples with coupling strength $C = 2.9$ and $C = 4.0$. The results are shown in Fig. 11. On the one hand, we calculated the mean value of both dimension \overline{D}_{BC} and \overline{D}_{KY} for the piecewise-smooth system with an increasing number of spins (solid lines), and on the other hand, we calculated the same values in the thermodynamic limit $N = \infty$ (dashed lines). For the piecewise-smooth system we take the average over 500 different realizations of the local disorder fields b_i at each value of N .

For $C = 4.0$ we can see, that both fractal dimensions of the piecewise-smooth system nearly converge to their values in the thermodynamic limit. This supports the assumption, that the piecewise-smooth system for a large number of spins behaves like its equivalent system in the thermodynamic limit. In contrast, for $C = 2.9$ the situation is not so clear. Even for $N = 20\,000$ the averaged values for the fractal dimension of the piecewise-smooth system are considerably different from the values in the thermodynamic limit. Remarkably, in the piecewise-smooth system the averaged Kaplan-Yorke dimension is smaller than one, which can be explained by the fact that for a nearly constant fraction of disorder realizations the system does not show chaos and $D_{KY} = 0$ [53].

For a more detailed analysis in this direction, we calculated the coefficient of variation, also often called Self-averaging Parameter (SAP) of the fractal dimensions, again for 500 different disorder realizations. The SAP is given by:

$$\text{SAP}[D] = \frac{\overline{D^2} - \overline{D}^2}{\overline{D}^2}. \quad (23)$$

In general, the SAP specifies the relative variance of a

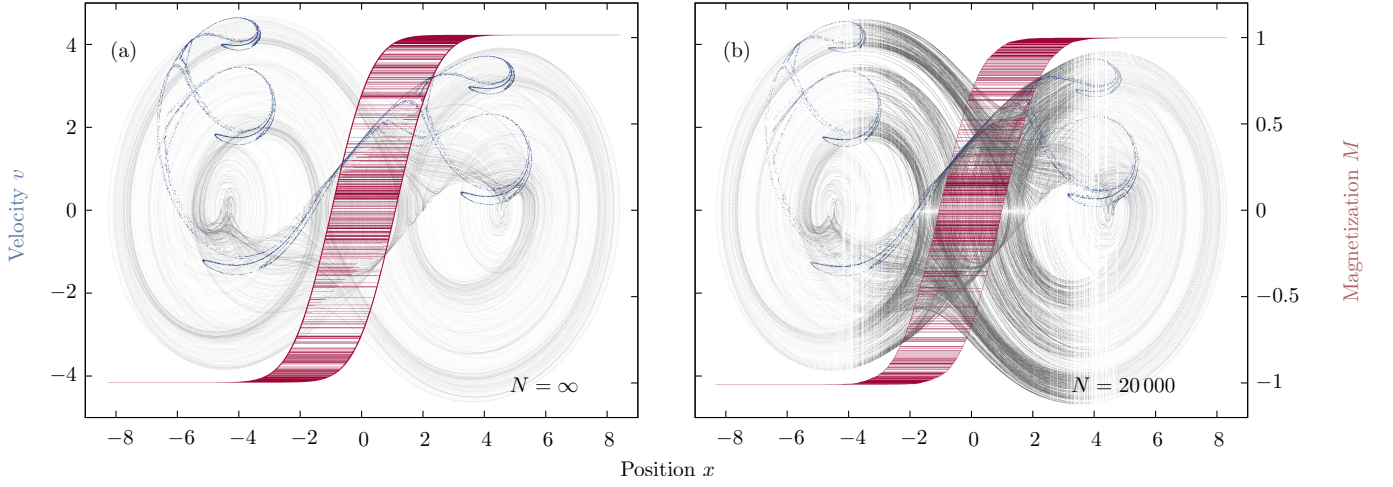


FIG. 10. Comparison of the chaotic attractor (—), the Poincaré section (—) and the magnetization (—). (a): The continuous system in its thermodynamic limit. (b): The piecewise-smooth system with $N = 20\,000$ spins. For both systems we chose $C = 4.0$ and one specific disorder realization b_i .

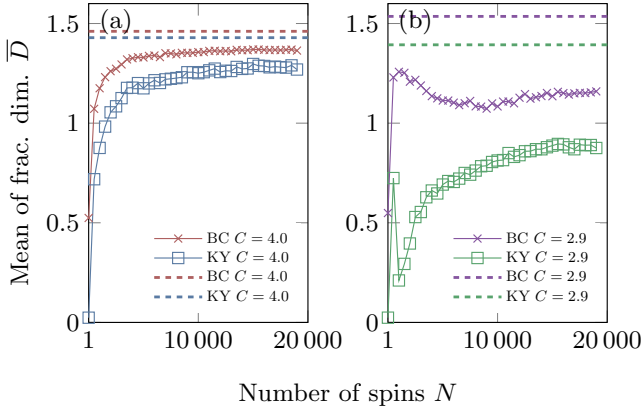


FIG. 11. Calculation of the mean of the box counting and the Kaplan-Yorke dimension over 500 disorder realizations for the piecewise-smooth system (squares and crosses). The dashed horizontal lines illustrate the corresponding fractal dimensions for the system in its thermodynamic limit. (a): The red and the blue curve are determined for $C = 4.0$ (—, —). (b): The green and violet curve for $C = 2.9$ (—, —).

quantity, here the fractal dimension. If it vanishes for $N \rightarrow \infty$, the behavior of the ensemble can be represented by only one realization of the local disorder with many spins. In Fig. 12 the $\text{SAP}[D]$ is illustrated in dependency on the number of spins for $C = 2.9$ and $C = 4.0$. One can see, that for $C = 4.0$ we have $\text{SAP}[D] \rightarrow 0$ for $N \rightarrow \infty$, which supports the argument that the fractal dimension converges to the value in the thermodynamic limit. More precisely, the $\text{SAP}[D]$ converges to zero in an algebraic way, whereas in the case of independent spins we found that $\text{SAP}[D]$ converges to zero in an exponential way [32]. A different behavior can be observed for $C = 2.9$. In this case, a constant value remains for $\text{SAP}[D]$, which means, that there is no self-averaging

and there are at least two or more different representative values of the fractal dimensions for the ensemble. In fact, for $C = 2.9$ and a large number of spins nearly 100 of the 500 disorder realizations lead to $D_{\text{KY}} = 0$ (see Figure 12(b)), whereas the remaining 400 realizations are associated with a Kaplan-Yorke dimension larger than one. This explains also the convergence of the averaged Kaplan-Yorke dimension \bar{D}_{KY} to a value between zero and one. Thus the thermodynamic limit $N = \infty$ and the limit of the piecewise-smooth system with large but finite N are different for $C = 2.9$, which strongly differs from the behavior that we found for independent spins [32].

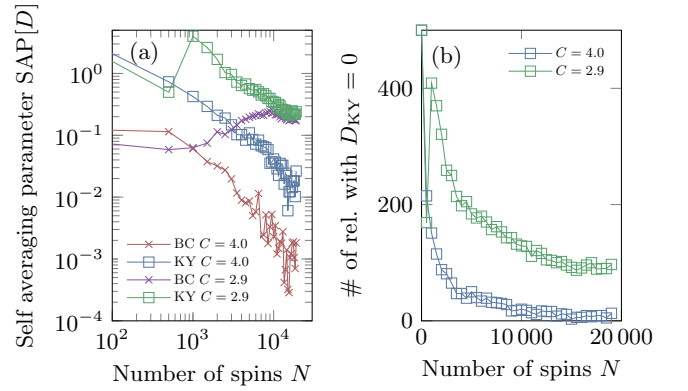


FIG. 12. (a): For $C = 4.0$ (—, —) and for $C = 2.9$ (—, —) we determined the SAP of the box counting and the Kaplan-Yorke dimension over 500 disorder realizations for the piecewise-smooth system. The fractal dimensions shows self averaging behavior in case of $C = 4.0$. For $C = 2.9$ the box counting and the Kaplan-Yorke dimension do not show self averaging properties. (b): For $C = 2.9$ the number of realizations with $D_{\text{KY}} = 0$ converges to a constant value near 100. This indicates the non self-averaging property of the Kaplan-Yorke dimension.

C. Magnetization

In addition to the fractal dimension we are interested in the behavior of the magnetization of the piecewise-smooth system. Since, in general, the mean of the magnetization becomes zero $\bar{M} = 0$, we calculated the variance of the magnetization instead of the SAP of the magnetization. The variance is defined by

$$\text{VAR}[M] = \overline{\left(\frac{1}{N} \sum_i \langle \sigma_i \rangle \right)^2} - \bar{M}^2, \quad (24)$$

where $\langle \sigma_i \rangle$ denotes the time-average of the configuration of the i th spin. Again the ensemble size for the quenched disorder is 500 and we have chosen $C = 2.9$ and $C = 4.0$. The results are shown in Figure 13. For $C = 2.9$ and

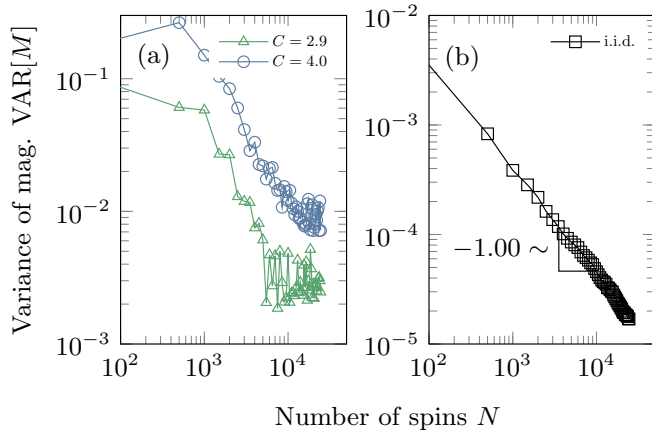


FIG. 13. (a): Variance of the magnetization in dependency on the the number of spins of the piecewise-smooth system for 500 disorder realizations. It can be seen, that for $C = 2.9$ and $C = 4.0$ the system does not self-average in reference to the magnetization. (b): Illustration of the variance of the magnetization for the system without dynamic feedback, but with iid input, here the variance of the the magnetization goes algebraically to zero with N^{-1} .

also for $C = 4.0$ we find, that up to $N \approx 5000$ and $N \approx 10000$, respectively, the variance of both system decreases roughly algebraically with N^{-1} . This behavior is equivalent to the behavior in a system without dynamic feedback but with Independent and Identically Distributed (iid) input, where the variance of the magnetization converges algebraically to zero in accordance with the central limit theorem. Instead in our coupled system, for a larger number of spins the decay of $\text{VAR}[M]$ becomes slower. This indicates, that for both values of C the magnetization does not show self-averaging. To verify the almost constant behavior of $\text{VAR}[M]$ for large N , we plotted the empirical Probability Density Function (PDF) in Fig. 14. For $C = 2.9$ (—) and $C = 4.0$ (—), we show the PDF, on the one hand, for $N = 10000$ and $N = 15000$ spins, respectively, and on the other hand, for $N = 20000$ spins. In addition, the behavior of

the PDF for iid input is shown (—). For the system with feedback the PDF of the magnetization becomes stationary for both values of C , whereas for the iid input the variance of the distribution decreases for an increasing number of spins N . This means, that for a large number of spins different time-averaged magnetizations are possible for different realizations of the local disorder field, which we have found already in the similar system with independent spins [32].

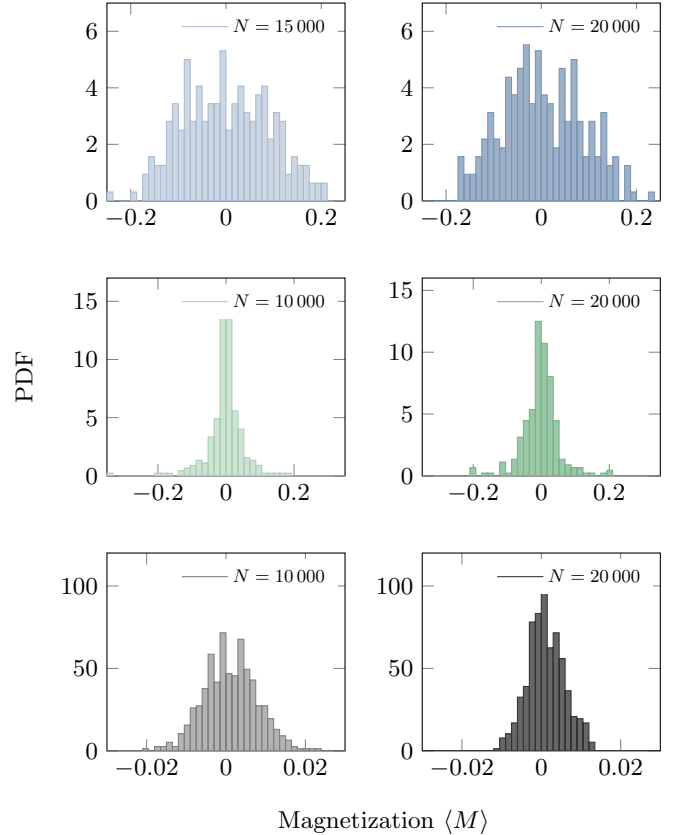


FIG. 14. Histograms of the empirical PDF for $N = 10000$, 15000 and 20000 for $C = 4.0$ (—), $C = 2.9$ (—) and for iid input (—). In contrast to the magnetization for iid input, in the system with feedback for both values of C the PDF does not become narrower for increasing N , which indicates the non self-averaging property of the magnetization.

V. CONCLUSION

In this paper we extended our results from the investigation of independent spins of a RFIM coupled to a damped and periodically driven harmonic oscillator [32] to pairwise interacting spins. We showed, that two interacting spins can form an elementary hysteresis loop, depending on the local disorder fields of the spins and the strength of the nearest neighbor interaction. We analyzed a system with hysteretic play character by using only loops with the same width. We determined the rela-

tionship between an ensemble of independent spin dimers at zero temperature and the Preisach operator and calculated the related Preisach density for the system in its thermodynamic limit.

From the numerically calculated bifurcation diagram for two spins, we showed that the behavior of few spins is very similar to the case of only one independent spin and typical bifurcation scenarios for piecewise-smooth system can be found. For a larger number of spins the bifurcation diagram is very similar to the bifurcation diagram of the system in its thermodynamic limit. In this case, obviously the typical bifurcation scenarios for grazing systems vanishes. We also compared the projected trajectories, the Poincaré sections and the magnetization curves for a typical chaotic attractors of the piecewise-smooth system and the system in its thermodynamic limit. We

found a good accordance between both systems. To determine how the dynamical properties of the system behaves for an increasing number of spins, we looked at the box counting and the Kaplan-Yorke dimension of the attractor for two different values of coupling strength. We found, that only in one of case the fractal dimensions of the attractors of the piecewise-smooth system converge to their value of the system in its thermodynamic limit. Also only in this case the system shows self-averaging in regard to the fractal dimensions. Furthermore we investigated the variance of the magnetization and found, that for both values of the coupling strength the variance does not converge to zero for increasing number of spins. In general from this we can suggest, that for a system with memory in form of a hysteretic play operator the limit $N = \infty$ and $N \rightarrow \infty$ are not necessarily equal.

-
- [1] N. S. Gusev, A. V. Sadovnikov, S. A. Nikitov, M. V. Sapozhnikov, and O. G. Udalov, Phys. Rev. Lett. **124**, 157202 (2020).
 - [2] V. K. Vlasko-Vlasov, U. Welp, A. E. Koshelev, M. Smylie, J.-K. Bao, D. Y. Chung, M. G. Kanatzidis, and W.-K. Kwok, Phys. Rev. B **101**, 104504 (2020).
 - [3] T. Moorsom, S. Alghamdi, S. Stansill, E. Poli, G. Teobaldi, M. Beg, H. Fangohr, M. Rogers, Z. Aslam, M. Ali, B. J. Hickey, and O. Cespedes, Phys. Rev. B **101**, 060408 (2020).
 - [4] G. Bertotti and I. D. Mayergoyz, *The science of hysteresis*, Vol. 1-3 (Academic Press, New York, 2006).
 - [5] G. Radons, Phys. Rev. Lett. **100**, 240602/1 (2008).
 - [6] H. Jiang, H. Ji, J. Qiu, and Y. Chen, IEEE Transactions on Ultrasonics, Ferroelectrics, and Frequency Control **57**, 1200 (2010).
 - [7] S. Schubert and G. Radons, Phys. Rev. E **96**, 022117 (2017).
 - [8] I. Urbanaviciute, T. D. Cornelissen, X. Meng, R. P. Sijbesma, and M. Kemerink, Nature Communications **9**, 4409 (2018).
 - [9] J. P. Sethna, K. Dahmen, S. Kartha, J. A. Krumhansl, B. W. Roberts, and J. D. Shore, Phys. Rev. Lett. **70**, 3347 (1993).
 - [10] M. P. Lilly, A. H. Wootters, and R. B. Hallock, Phys. Rev. Lett. **77**, 4222 (1996).
 - [11] P. Shukla, Phys. Rev. E **62**, 4725 (2000).
 - [12] S. Sabhapandit, D. Dhar, and P. Shukla, Phys. Rev. Lett. **88**, 197202 (2002).
 - [13] J. M. Deutsch, A. Dhar, and O. Narayan, Phys. Rev. Lett. **92**, 227203 (2004).
 - [14] J. M. Goncalves, A. Megretski, and M. A. Dahleh, IEEE Transactions on Automatic Control **46**, 550 (2001).
 - [15] Z. T. Z., E. M., V. G. R., and R. A. N., Physica D: Nonlinear Phenomena **306**, 6 (2015).
 - [16] J. Sieber, Nonlinearity **19**, 2489 (2006).
 - [17] F. Preisach, Zeitschrift für Physik **94**, 277 (1935).
 - [18] I. D. Mayergoyz, *Mathematical models of hysteresis and their applications* (Academic Press, New York, 2003).
 - [19] M. Ruderman, F. Hoffmann, and T. Bertram, IEEE Transactions on Industrial Electronics **56**, 3840 (2009).
 - [20] H. Lamba, M. Grinfeld, S. McKee, and R. Simpson, IEEE Trans. Magn. **33**, 2495 (1997).
 - [21] A. Rezaei-Zare, M. Sanaye-Pasand, H. Mohseni, S. Farhangi, and R. Iravani, IEEE Trans. Power Delivery **22**, 919 (2007).
 - [22] G. Radons and A. Zienert, Eur. Phys. J. Special Topic **222**, 1675 (2013).
 - [23] K. Kuhnen and H. Janocha, in *1999 European Control Conference (ECC)* (1999) pp. 791–796.
 - [24] M. Ruderman, S. Yamada, and H. Fujimoto, Journal of Dynamic Systems, Measurement, and Control **141** (2019).
 - [25] A. Visintin, *Differential Models of Hysteresis*, Applied Mathematical Sciences (Springer Berlin Heidelberg, 2013).
 - [26] P. Krejčí and K. Kuhnen, IEE Proc. Control Theory Appl. **148**, 185 (2001).
 - [27] L. Riccardi, D. Naso, B. Turchiano, and H. Janocha, IEEE Transactions on Control Systems Technology **22**, 1268 (2014).
 - [28] Y. Imry and S. Ma, Phys. Rev. Lett. **35**, 1399 (1975).
 - [29] O. Perkovic, K. A. Dahmen, and J. P. Sethna, Phys. Rev. Lett. **75**, 4528 (1995).
 - [30] P. Shukla, Physica A **233**, 235 (1996).
 - [31] J. P. Sethna, K. A. Dahmen, and C. R. Myers, Nature **410**, 242 (2001).
 - [32] P. Zech, A. Otto, and G. Radons, Phys. Rev. E **101**, 042217 (2020).
 - [33] E. Vives, M. L. Rosinberg, and G. Tarjus, Phys. Rev. B **71**, 134424 (2005).
 - [34] F. Salvat-Pujol, E. Vives, and M. L. Rosinberg, Phys. Rev. E **79**, 061116 (2009).
 - [35] K. Dahmen and J. P. Sethna, Phys. Rev. B **53**, 14872 (1996).
 - [36] M. Brokate and J. Sprekels, *Hysteresis and phase transitions* (Springer, New York, 1996).
 - [37] M. Dimian and P. Andrei, *Noise-Driven Phenomena in Hysteretic Systems*, Signals and Communication Technology (Springer New York, 2013).
 - [38] M. di Bernardo, C. Budd, A. R. Champneys, and P. Kowalczyk, *Piecewise-smooth Dynamical Systems: Theory and Applications*, Applied Mathematical Sciences, Vol. 163 (Springer London, 2008).

- [39] J. M. Goncalves, A. Megretski, and M. A. Dahleh, IEEE Transactions on Automatic Control **46**, 550 (2001).
- [40] S. Theodossiades and S. Natsiavas, Journal of Sound and Vibration **229**, 287 (2000).
- [41] U. Galvanetto, Journal of Sound and Vibration **248**, 653 (2001).
- [42] X. Zhao and H. Dankowicz, Journal of Computational and Nonlinear Dynamics **1**, 109 (2006).
- [43] I. D. Mayergoyz, *Mathematical models of hysteresis* (Springer, New York, 1991).
- [44] A. B. Nordmark, Journal of Sound and Vibration **145**, 279 (1991).
- [45] P. C. Müller, Chaos, Solitons & Fractals **5**, 1671 (1995).
- [46] H. Dankowicz and A. B. Nordmark, Physica D: Nonlinear Phenomena **136**, 280 (2000).
- [47] M. di Bernardo, C. J. Budd, and A. R. Champneys, Phys. Rev. Lett. **86**, 2553 (2001).
- [48] C. Budd and F. Dux, Nonlinearity **7**, 1191 (1994).
- [49] W. Chin, E. Ott, H. E. Nusse, and C. Grebogi, Phys. Rev. E **50**, 4427 (1994).
- [50] S. Foale and S. R. Bishop, Nonlinear Dynamics **6**, 285 (1994).
- [51] H. G. E. Hentschel and I. Procaccia, Physica D: Nonlinear Phenomena **8**, 435 (1983).
- [52] P. Grassberger and I. Procaccia, Physica D: Nonlinear Phenomena **9**, 189 (1983).
- [53] For a regular behavior of the system, the largest Lyapunov exponent $\lambda_1 = \lambda_{\max} = 0$ associated to perturbations of the phase of the external forcing. However, these perturbations are neglected here, leading to $\lambda_{\max} < 0$ and $D_{KY} = 0$.